An Investigation of Late-Combustion Soot Burnout in a DI Diesel Engine using Simultaneous Planar Imaging of Soot and OH Radical

John E. Dec
and
Peter L. Kelly-Zion
Sandia National Laboratories

INTRODUCTION

Diesel engine design continues to be driven by the need to improve performance while at the same time achieving further reductions in emissions. The development of new designs to accomplish these goals requires an understanding of how the emissions are produced in the engine. Laser-imaging diagnostics are uniquely capable of providing this information, and the understanding of diesel combustion and emissions formation has been advanced considerably in recent years by their application [1]. However, previous studies have generally focused on the early and middle stages of diesel combustion, and there is little detailed understanding of the late stages and the mechanism whereby soot escapes oxidation to become a tail-pipe emission.

These previous laser-imaging studies do, however, provide important insight into the soot formation and oxidation processes during the main combustion event [1]. They indicate that prior to the end of injection, soot formation is initiated by fuel-rich premixed combustion (equivalence ratio > 4) near the upstream limit of the luminous portion of the reacting fuel jet. The soot is then oxidized at the diffusion flame around the periphery of the luminous plume. Under typical diesel engine conditions, the diffusion flame does not burn the remaining fuel and soot as rapidly as it is supplied, resulting in an expanding region of rich combustion products and soot. This is evident in natural emission images by the increasing size of the luminous soot cloud prior to the end of injection (see for example Refs. [2,3]). Hence, the amount of soot in the combustion chamber typically increases until shortly after the end of fuel injection, at which time the main soot formation period ends and the "burnout" phase begins. Sampling valve and two-color pyrometry data indicate that the vast majority (more than 90%) of the soot formed is oxidized before combustion ends; however, it is generally thought that a small fraction of this soot from the main combustion zones is not consumed and is the source of tailpipe soot emissions [2].

Natural-luminosity images have also provided support for this hypothesis that incomplete soot burnout in the bulk gases (*i.e.* not near the cylinder or combustion-bowl walls) is likely to be the source of tail-pipe soot emissions. They show pockets of luminous soot persisting in the bulk gas after the main combustion event, with the signal becoming progressively weaker until it is no longer detectable. However, it should be noted that there may be other mechanisms whereby soot escapes combustion. Kittelson [4] presented data from an older (1981) smaller-bore diesel engine which indicated that a large fraction of the emitted soot had been in contact with the combustion chamber walls, before entering the exhaust stream. It is unclear if these results are relevant to a modern heavy-duty diesel engine, but they suggest that wall flame-quench followed by wall soot-deposition and subsequent blow-off is a possible alternative pathway for soot emissions. Another potential pathway is soot being forced into the ring crevices near TDC (top dead center) and being released late in the expansion or during the exhaust stroke. Finally, it is possible that more than one pathway contributes to the total soot emissions.

In the current work, we more fully investigate the pathway of incomplete soot burnout in the bulk gases during the late stages of diesel combustion by simultaneously imaging the OH-radical and soot distributions using planar laser-

DISCLAIMER

DISCLAIMER

Portions of this document may be illegible in electronic image products. Images are produced from the best available original document.

induced fluorescence (PLIF) and planar laser-induced incandescence (PLII), respectively.[1] OH radicals are generated in the near stoichiometric and lean combustion zones (typically in diffusion flame zones) and persist in the post-combustion gases as long as the local gas temperature remains sufficiently high. Accordingly, during the late stages of combustion, the OH radical distribution marks the reaction-zones and regions where products are sufficiently hot for significant soot oxidation to occur. The presence of OH can also be important because OH-radical attack is thought to be a major mechanism for soot oxidation, particularly in fuel-rich and near-stoichiometric products [2]. Images of the soot distribution show where soot remains during the late stages of diesel combustion, and simultaneous images of the OH and soot show their relative locations, allowing the potential for oxidation of the remaining soot to be assessed.

The measurements in the current study were made in an optically accessible direct-injection (DI) diesel engine of the heavy-duty size class. Detailed descriptions of this engine, the operating conditions, diagnostics, and optical setup are given in the next section. Following this, the understanding of DI diesel combustion obtained from previous laser-imaging studies is briefly reviewed as a starting point for the current study. Then, the main results of the current study are presented and discussed. Because engine-out soot emissions can vary widely with engine operating parameters, measurements were made for several operating conditions, including variations in injection timing, engine speed, fuel loading, and diluent level. Temporal sequences of simultaneous OH and soot images are presented and discussed for each of these conditions along with a comparison of the in-cylinder soot data with exhaust-emission measurements. In the final section, the article is summarized and conclusions are drawn.

[1] PLII was selected over the more easily implemented elastic-scatter soot imaging because it has two major advantages: 1) the signal is, to first order, proportional to the soot volume (d^3) so PLII images give a more accurate picture of the soot distribution, and 2) laser light scattered off in-cylinder surfaces and liquid fuel is easily rejected.

EXPERIMENT AND DIAGNOSTICS

The optical-access engine used in this investigation was a single-cylinder, direct-injection, 4-stroke diesel engine based on a Cummins N-series production engine. The N-series engine is typical of heavy-duty size-class diesel engines, with a bore of 140 mm and a stroke of 152 mm. These dimensions are retained in the optical-access engine, and a production Cummins N-series cylinder head is used so that the production-engine intake port geometry is also preserved. The in-cylinder flow field of a similar Cummins N-series research engine has been examined under motored conditions and found to be nearly quiescent [5]. To provide optical access, the engine is equipped with a classic extended piston and piston-crown window. This piston-crown window provides a full view of the combustion bowl and was used to acquire all the images presented in this article. Additional windows located around the top of the cylinder wall provide the orthogonal optical access required for planar imaging. Figure 1 presents a generalized schematic of this engine, and a complete description of the engine may be found in Ref. [3].

This research engine is equipped with a Cummins CELECT™ electronic fuel injector. This closed-nozzle unit injector uses camshaft actuation to build injection pressures. Typically, this engine operates with an 8-hole (equally spaced at 45°) tip; however, for the experiments presented here, the injector was equipped with a custom 7-hole tip. The hole spacing on this tip was the same as that of the 8-hole tip (45°) except that the hole opposite the imaged jet was missing, leaving a 90° gap between holes. This allowed the laser sheet to reach the imaged fuel jet without attenuation from the opposing jet. The nominal nozzle-hole diameter for the original 8-hole tip is 0.194 mm, and the nominal angle of the fuel-jet axis is 14° downward from horizontal. This same hole size was maintained for five holes in the 7-hole tip, but the two holes adjacent to the "missing" eighth hole were enlarged to a diameter of 0.238 mm to maintain the same total fuel flow rate as the standard tip. Thus, the measurements reported in this paper were made in a sector of the cylinder supplied by an unaltered jet, and the jets adjacent to the imaged sector were also unaltered.

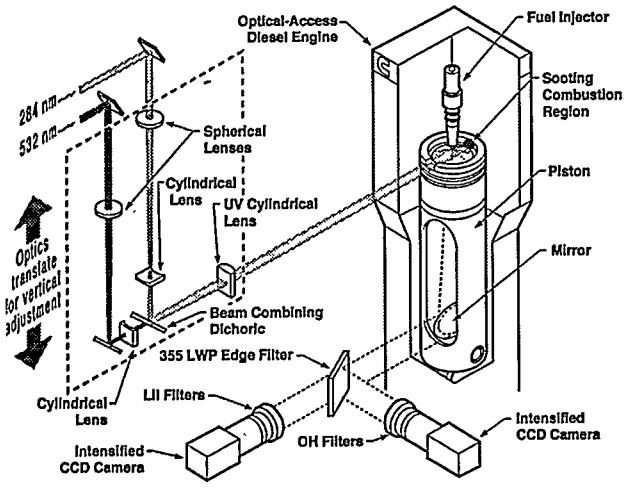

Figure 1. Schematic of the optical-access diesel engine showing the optical setup for simultaneous OH-PLIF and PLII-soot imaging.

All experiments were conducted with Phillips No. 2 diesel fuel (D2) at a representative diesel-engine operating condition corresponding to a motored TDC temperature and pressure of 992 K and 5.0 MPa, respectively. Before conducting the experiments the engine was heated to 368 K (95° C) by means of electrical heaters on the "cooling" water and lubricating oil circulation systems. To minimize the rate of window fouling and to avoid overheating, the engine was fired once every 10th engine cycle, at which time the data were acquired. Measurements were made for both normal (11.5° BTDC) and 11.5°-retarded (TDC) injection timing at four different combinations of fuel load, engine speed, and N_2-diluent levels, as summarized in Table 1. This amount of timing retard is typical of amounts used to control NO_X. Nitrogen was used as an inert diluent to simulate the effect of EGR (exhaust gas recirculation) which is also used to reduce NO_X emissions. For convenience, the fuel loading is stated in terms of a charge/fuel (C/F) ratio, which is the same as the air/fuel (A/F) ratio when no N_2 is added. With N_2 addition, the air/fuel ratio is slightly less, as noted in Table 1.

A dual-laser, dual-camera system was used to obtain the simultaneous "single-shot" images, as shown schematically in Fig. 1. The OH PLIF laser was tuned to a strong feature of the A-X, (1,0) transition at 284.01 nm. This line was selected for its high fluorescence yield and because it is relatively insensitive to temperature

TABLE 1. Engine Operating Conditions

Motored TDC pressure	5.0 MPa
Estimated motored TDC temperature	992 K
Estimated motored TDC density	16.6 kg/m^3
Normal Timing – Start of Injection	11.5° BTDC
Retarded Timing – Start of Injection	TDC
Base Condition: Medium-Low Fuel Load – Medium Speed	
Engine speed	1200 rpm
Charge/Fuel Ratio (mass basis)	65
Fuel injected per cycle	0.079 ml
N_2 Diluent	0%
High Fuel Load - Medium Speed	
Engine speed	1200 rpm
Charge/Fuel Ratio (mass basis)	31
Fuel injected per cycle	0.152 ml
N_2 Diluent	0%
High Fuel Load - High Speed	
Engine speed	1680 rpm
Charge/Fuel Ratio (mass basis)	31
Fuel injected per cycle	0.152 ml
N_2 Diluent	0%
High Fuel Load - High Speed – 10% N_2 diluent	
Engine speed	1680 rpm
Charge/Fuel Ratio (mass basis)	31
Air/Fuel Ratio (mass basis)	28
Fuel injected per cycle	0.152 ml
N_2 Diluent (molar fraction of intake gas)	10%

variations over the range of interest. The output of this laser was about 22 mJ per pulse prior to entering the cylinder, and it was monitored to insure that the energy stayed within ±10% of this value, since the OH-PLIF signal can vary with laser energy. The PLII signal was produced using a frequency-doubled Nd:YAG laser at 532 nm whose output was about 120 mJ prior to entering the cylinder. This pulse energy is sufficiently high to make the PLII signal insensitive to laser-energy fluctuations [6], which were less than ±5% in this study.

The two laser beams were combined into overlapping laser sheets approximately 25 mm wide and 0.2 mm and 0.3 mm thick for the PLIF and PLII lasers, respectively, using a combination of lenses and a dichroic reflector (see Fig. 1). The combined beams were directed into the combustion chamber through one of the windows at the top of the cylinder wall which was opposite the region of the imaged

fuel jet, and inline with the "missing" fuel jet of the 7-hole injector described above. Images were acquired through the piston-crown window with the OH and soot signals being separated into the two intensified video cameras by means of an edge filter. Each camera was equipped with additional filters to isolate the appropriate signal.

To prevent cross-talk between the two images, the laser Q-switch timing was adjusted so that the OH PLIF laser fired 200 ns prior to the PLII laser, and the camera gatewidths were set to 110 ns and 70 ns, respectively, with the laser pulses centered in the camera gates. This 200 ns delay time is negligible for any fluid mechanics or soot burnout rates, so it should have no effect on the apparent simultaneity of the images. For each crankangle at each operating condition, a minimum of 12 (and more typically 24) image pairs were acquired for 12 or 24 separate fired cycles. The images presented have been subjectively selected from these sets.

DIESEL COMBUSTION PRIOR TO LATE-COMBUSTION SOOT BURNOUT

Previous work involving several different laser imaging diagnostics has carefully detailed the events that occur during the ignition delay, start of combustion, premixed burn, and the mixing controlled burn including the transition to the quasi-steady period [1,7,8]. Figure 2, reproduced from Ref. [1], presents an idealized schematic showing the main features of a reacting diesel fuel jet during the quasi-steady period, *i.e.* the period after the initial premixed burn until the end of fuel injection. As discussed in detail in these references, the high injection velocity causes high rates of air entrainment into the jet and keeps the diffusion flame lifted. Thus, combustion is thought to occur in two stages: first as a very rich ($\phi > 4$) premixed reaction which leads to the initial soot formation; then second, the products of the rich premixed combustion burn out as a near-stoichiometric diffusion flame at the jet periphery. The soot particles travel along with the other rich-combustion products to the diffusion flame where they burn out due to the high temperatures and the availability of OH-radicals and/or oxygen. The exact nature of the soot

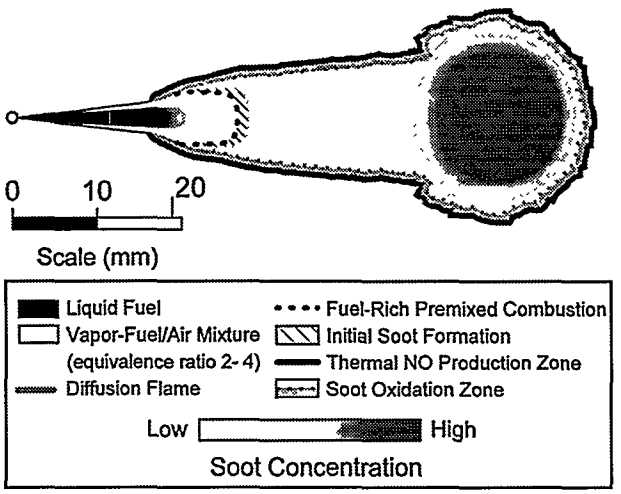

Figure 2. A schematic showing the features of a reacting diesel fuel jet at a typical time during the quasi-steady portion of combustion, *i.e.* after the initial pre-mixed burn through the end of fuel injection. Reproduced from Ref. [1].

oxidizing reactions is not known, but OH-radical attack is thought to be a major mechanism, particularly in fuel-rich and near stoichiometric products [2]. Finally, it should be noted that in a real engine, the jet reaches the combustion bowl wall during the quasi-steady period[2] and the idealized schematic in Fig. 2 will become distorted as the leading portion spreads out along the wall.

Although the events occurring after fuel injection ends have been less well studied, sufficient data exists to at least generally understand the transition from the quasi-steady period to the later burnout stages that are the main subject of the work in this article. Natural flame luminosity [3,7], and PLII and elastic-scatter soot [1] image sequences show that when fuel injection ends, combustion quickly spreads back to the injector, with soot forming in this upstream region as well. Thus, the flame standoff and premixed reaction zone disappear, and the reacting jet consists of the sooty products of rich premixed combustion (along with some diffusion-flame products) completely surrounded by a diffusion flame. Then, the jet-like nature of the soot-filled combusting region gradually disappears as the upstream portion (the part ex-

[2] For small-bore (automotive size) diesels, the jet can reach the wall prior to the quasi-steady period.

tending up to the injector) is gradually carried downstream by its remaining momentum to the leading portion of the jet which is spreading out along the combustion-bowl wall. Momentum from the injection process continues to spread this soot-filled combusting region along the bowl wall until it encounters the remains of the adjacent jet and then folds back toward the center of the bowl. As this process proceeds, oxidation reduces the size of this region, and this initially intact region breaks into separate, smaller "pockets" of combustion. Although the number and location of these luminous pockets vary from cycle to cycle, quite often there are initially two distinct pockets in the remains of the wings of the jet (as seen in the images presented below) due to the residual flow pattern of the jet. As the burnout continues, the remaining pockets continue to get smaller, sometimes breaking into two or more smaller pockets, and eventually they lose any obvious spatial correlation to the original combusting fuel jet.

SIMULTANEOUS OH AND SOOT IMAGES

Details of the laser sheet location and field of view for the simultaneous OH and soot images are shown in Fig. 3. As indicated in Fig. 1, the entire sheet-forming lens and mirror assembly is mounted on a translation stage so that the combined laser sheets can be adjusted vertically to various positions below the cylinder head, as shown in Fig. 3a. However, the size of the cylinder-wall window limits the lowest elevation of a horizontal laser sheet to about 36 mm below the cylinder head. As will be discussed with the data presentation, it was necessary to position the laser sheet lower for investigation of the high fuel-load condition. This was accomplished by angling the laser sheet downward at approximately an 8.5° angle so that it was 53 mm below the cylinder head in the center of the field of view as shown in Fig. 3b. With this setup the laser sheet elevation varies a few millimeters across the field of view. Figure 3c shows the field of view for the images which were acquired through the piston-crown window. The field of view in Fig. 3c is shown with the piston in the TDC position; however, as the piston moves down well below the laser sheet, the parallax is such that the piston no longer blocks the field of view on the right as indicated in Fig. 3c.

Medium-Low Load (C/F = 65), 1200 rpm Condition

Figure 4 presents temporal sequences of simultaneous OH and soot images for both normal and 11.5°-retarded timing at the medium-low load (C/F = 65), 1200 rpm condition. For all the images presented in this paper, 0° crankangle (CA) is defined as TDC exhaust, so

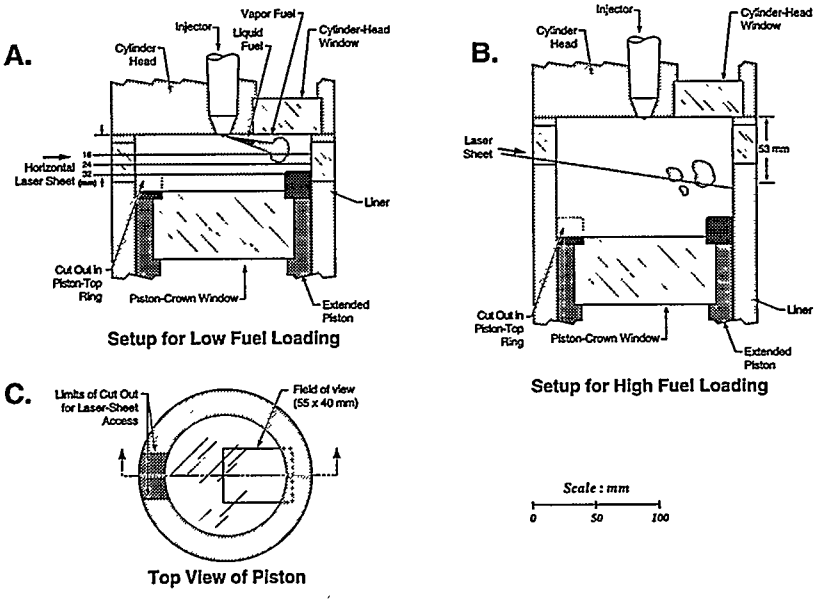

Figure 3. Detailed schematic of the combustion chamber showing the laser sheet orientation and field of view.

TDC compression is at 360°. Fuel injection starts at 348.5° (11.5° BTDC) and 360° (TDC) for the normal and retarded timing cases, respectively, as noted in Table 1. The small white dot near the left edge of each image marks the location of the injector, and the curve at the right shows the edge of the combustion bowl when the piston is in the TDC position.

Both the OH and soot images were originally obtained as gray-scale intensity maps on separate cameras as shown in Fig. 1. In order to view the spatial relationship between the OH and soot fields, it is necessary to superimpose the two images while maintaining a distinction between the two fields. The best method of doing this is to use a different false color mappings for each of the two fields Accordingly, the superposition was originally accomplished by mapping the OH distribution to shades of green and the soot to shades of red, with the overlap regions appearing as yellow. For the current article, it was necessary to make a black and white version of these superimposed images. Several different gray-scale mappings were evaluated before selecting the one used in Figs. 4-7. As noted in the legend at the top of each figure, the soot regions are shown as black, while the OH distribution is shown in shades of gray from a medium-gray to white. The overlap regions show as darker gray; however, there is some ambiguity between higher-intensity OH signal overlapped with soot and low-intensity OH signal near the edges of the OH distribution. The current scheme also does not show the intensity variation of the PLII-soot signal. Attempts to show the soot in shades of dark gray produced confusion between soot, soot and OH overlap regions, and low-intensity OH. Despite these shortcomings, most essential information is still discernable in the images presented here.

As shown in Fig. 3, the laser sheets propagate from left to right, and they were positioned in three different image planes to obtain the sequences in Fig. 4, as noted at the top of each image. This was necessary because, during the burnout phase of combustion, the main combusting region moves down with the piston, presumably as a result of residual downward momentum from the 14° downward angle of the

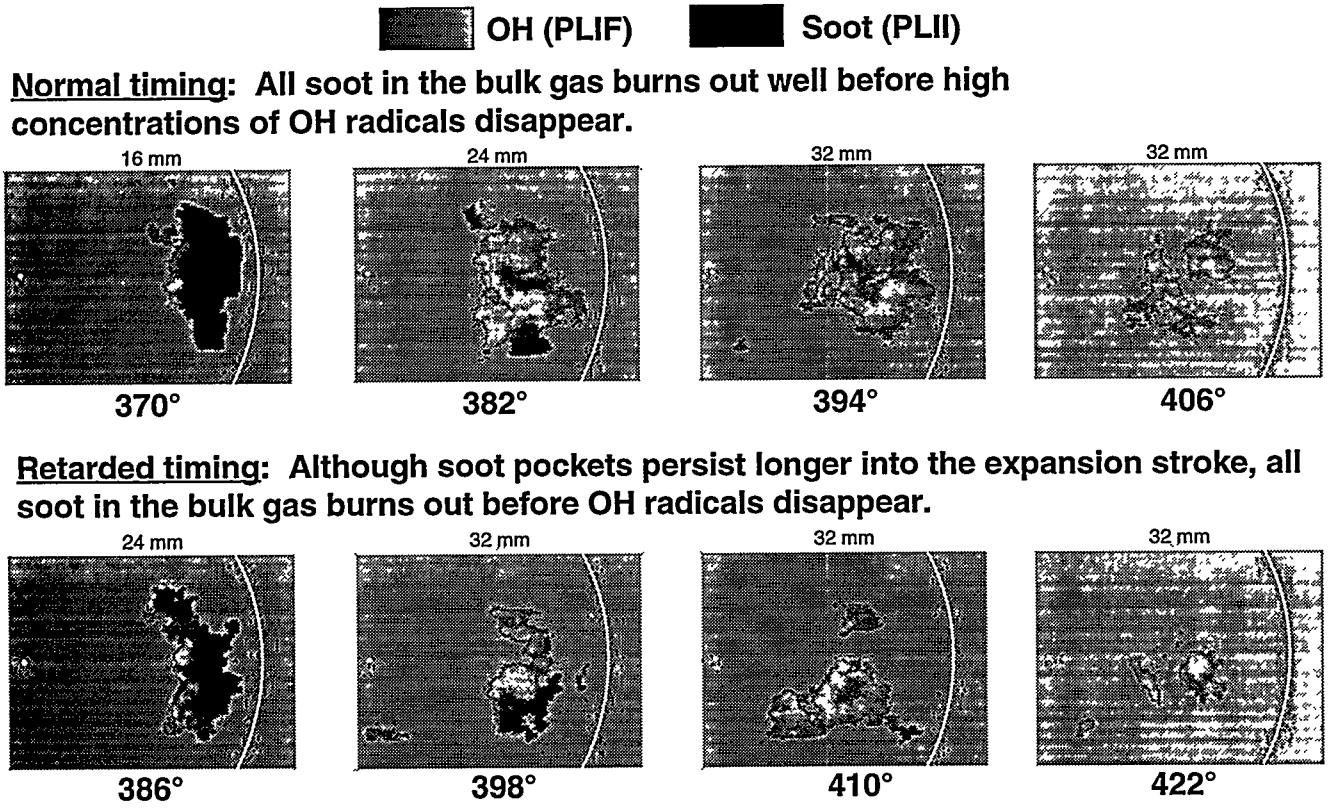

Figure 4. Temporal sequences of simultaneous OH and soot images at normal and 11.5°-retared injection timing for the case of medium-low load (C/F = 65), 1200 rpm.

injector holes. Note that the first images of the sequences in Fig. 4 are in the 16 and 24 mm image planes for the normal and retarded timing, respectively because the combustion zone has moved downward for the retarded-timing case, since it occurs later. Note that the images for the retarded-timing sequence in Fig. 4 are taken 16° CA later than those in the normal-timing sequence. However, other than this shift in location and timing, the sequences for two injection timings are quite similar for this C/F = 65, 1200 rpm case.

By the start of the image sequences in Fig. 4, the jet-like nature of the combustion has disappeared and the sooty-combustion region is confined to the outer part of the combustion bowl. The combined OH and soot images show a broad soot region with a thin layer of OH-radicals along the left edge, indicating that a diffusion flame still surrounds this remaining soot region, as it did during the earlier stages of combustion depicted in Fig. 2. It should be noted that both the OH and the soot fields are truncated at the top and bottom of the image because the field of view is greater than the laser-sheet width. The truncation of the OH image is more severe since the OH signal is more sensitive to the reduced laser intensity toward the edges of the sheet. As a result, soot often appears to extend beyond the OH at the top and bottom of the images as seen in the 370° and 382° images of the normal-timing sequence in Fig. 4. In addition, the lasers are attenuated by the soot cloud, so it cannot be determined how far the large soot region in the first image of each sequence extends to the right; however, luminosity images suggest that it extends to (or nearly to) the bowl wall [7]. Attenuation is more severe for the retarded-timing case indicating higher soot levels within the soot cloud.

Then, for both cases, the single, large soot area breaks into smaller pockets that have moved out into the bulk gas, away from the wall. Combustion and soot oxidation are also occurring as the soot regions become smaller and eventually disappear. These soot pockets are surrounded by a region of OH indicating the presence of a diffusion flame, and as the burnout progresses, OH is also broadly distributed through the surrounding gases. This broadly distributed "bulk-gas" OH indicates the presence of combustion product gases that are still at or above 1900 to 2000 K, which is sufficiently hot for soot oxidation to occur. The presence of the OH radical itself might also play a role in the soot oxidation as discussed in the introduction. Thus, even if the diffusion flame were to go out, the remaining soot would almost certainly be oxidized in these hot gases. By the end of the sequences, all the soot has disappeared, and there is still substantial OH signal.

To verify that there was no remaining soot at other elevations, the laser sheet was moved above and below the three image planes reported in Fig. 4. Like the images in Fig. 4, they showed no unburned bulk-gas soot at this operating condition, even with retarded timing. Therefore, no engine-out soot emissions would be expected unless they result from a different mechanism. This is in agreement with Bosch smoke measurements that showed virtually no exhaust soot for this C/F = 65, 1200 rpm operating condition for either injection timing. It is also in agreement with typical production-engine data which show very low particulates at lower-load, lower-speed conditions.

High-Load (C/F = 31), 1680 rpm Condition

Production engines typically produce higher soot emissions at higher-load, higher-speed conditions, particularly when injection timing is retarded to reduce NO_X emissions. Figure 5 shows the results of simultaneous OH and soot imaging for a high load (C/F = 31), 1680 rpm condition. With this higher fuel loading, the combustion period is considerably longer, and it persists farther into the expansion stroke. Because the main combustion regions follow the piston down, it was necessary to lower the laser to an elevation of 53 mm below the cylinder head using the laser sheet orientation shown in Fig. 3b. With this low laser-sheet position, the piston has not moved below the plane of the laser until just before 420°, which is the starting crankangle of the image sequences in Fig. 5.

The first image (420°) of the normal-timing sequence is similar to the later soot burnout images in Fig. 4. There are only a few small pockets of soot remaining, and they are surrounded by a broad region of strong OH signal. This indicates that these remaining soot pock-

ets are still actively burning, and that even if the diffusion flames around these pocket were to go out, any remaining soot would almost certainly be oxidized in the surrounding hot-product gases. Both the OH and soot signals then fall off rapidly through the rest of the sequence with no detectable signal beyond 480°. We believe that this occurs because the remaining pockets of soot and vapor-phase fuel are consumed, ending the heat-producing reactions, and the rapid expansion at these crankangles quickly cools the hot-product gases. Except for a few very small pockets of soot at 460° and 480° that may not be completely consumed, the bulk-gas soot burns out and is not a source of exhaust soot emissions for normal timing.

However, for retarded timing at this higher-speed, high-load condition, the bulk-gas soot burnout is much less complete, as evident in Fig. 5. There are still large pockets of soot present when the exhaust valve opens (EVO) at 490°. In some cycles, these soot pockets are still surrounded by diffusion flames as in the 480° image; however, it is unlikely that these relatively large soot pockets will be completely consumed before they flow out the exhaust valve. In other cycles, the combustion reactions have nearly gone out, or gone out completely as evident in the 500° image. It is noteworthy that even when these soot pockets are actively burning (480° image), there are no broad regions of OH outside the diffusion flame zone. This indicates that by these late crankangles, the bulk gases have cooled below temperatures that would support soot oxidation, so when the diffusion flame goes out, all soot oxidation will cease. Thus, these images indicate that incomplete soot burnout in the bulk gases is likely to be a significant source of tail-pipe soot emissions for retarded timing at this 1680 rpm, high-load condition.

N_2 Diluent Addition at the High-Load (C/F = 31), 1680 rpm Condition

The addition of inert diluents (typically via EGR) is another method of reducing combustion temperatures to reduce NO_X emissions. However, EGR addition has often been associated with increased soot emissions in prototype engine tests. In order to investigate the effects of inert diluents on the bulk-gas soot burnout, the study

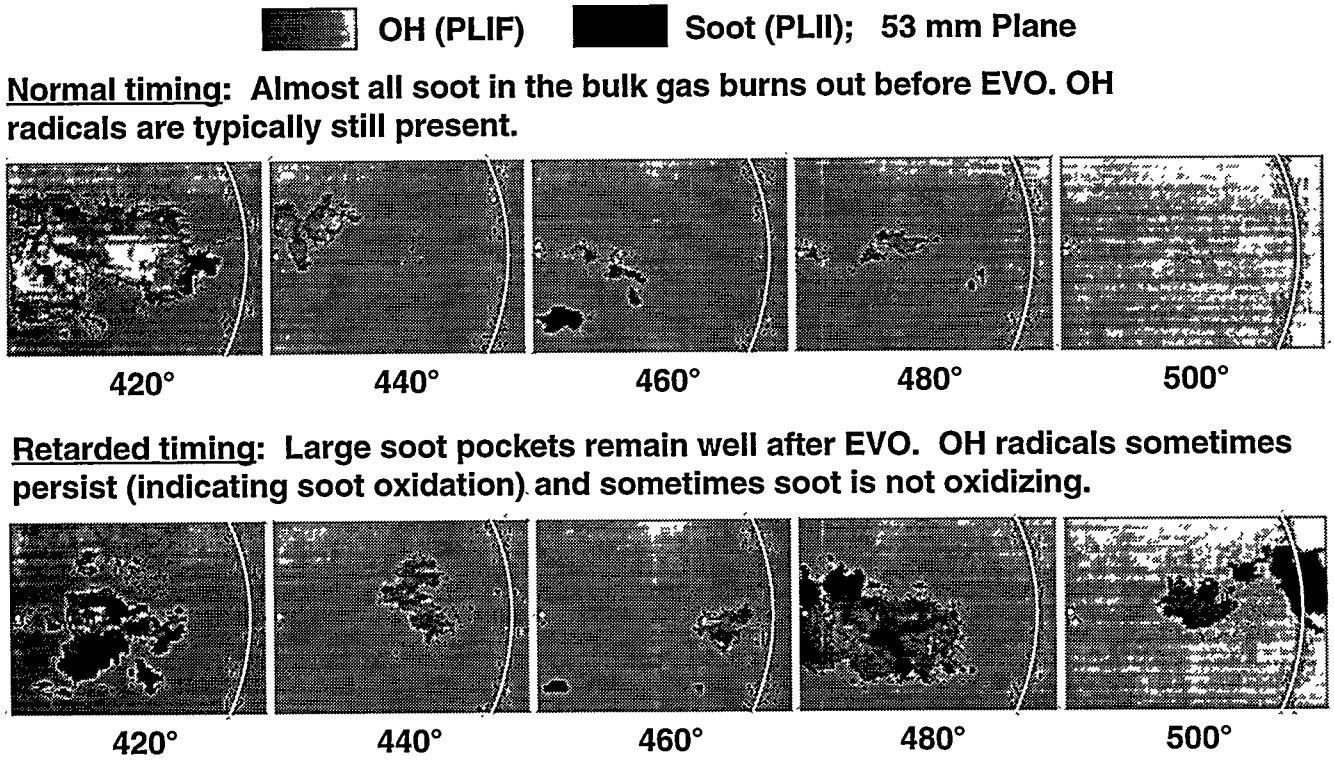

Figure 5. Temporal sequences of simultaneous OH and soot images at normal and 11.5°-retarded injection timing for the case of high load (C/F = 31), 1680 rpm.

presented in Fig. 5 (high-load, 1680 rpm) was repeated with 10% N_2 added to the intake air (molar basis). The addition of this nitrogen reduced the air/fuel ratio to 28; however this slightly lower A/F ratio is thought to have only a small (~10%) effect on soot emissions for two reasons. First, the addition of 10% N_2 has almost no effect (0.5° shift) on the apparent heat release rate curve, indicating a minimal change in the fuel-air mixing rate. Second, emission measurements from a near production version of our research engine showed only about a 10% increase in particulate emissions as the A/F was reduced from 30.7 to 27.5, as is typical of data from other engines. In contrast, adding 10% N_2 reduces the flame and post-combustion gas temperatures by 100 to 200 K. This will have a significant impact on reaction rates and on concentrations of radicals such as OH, which tend to be exponential in temperature.

Figure 6 shows the effect of 10% N_2 diluent on the late-combustion soot burnout for normal injection timing at the high-load (C/F =31), 1680 rpm condition. The 0% N_2 image sequence from Fig. 5 is re-presented here so that the changes with 10% N_2 diluent are more easily seen. These images show that the addition of the diluent significantly increases the amount of soot remaining during the late stages of combustion. At 420° two large pockets of soot are present in the image shown. OH is also present around the sooting region and distributed throughout the region between the two soot pockets. However, both the extent of the OH distribution and the intensity of the OH signal are significantly less than for 0% N_2 at 420°.

Although other factors can affect the OH-PLIF signal intensity besides OH concentration, these parameters vary only slightly between the 0% and 10% N_2 cases. A full discussion of these factors which include temperature, density, line broadening, and collisional partners, is beyond the scope of this article. However, estimates show that they will have only a 10-20% effect on the OH-signal intensity between these two cases. Also, for all operating conditions, expansion of the in-cylinder gases through a temporal sequence will increase the signal for a given OH concentration, mainly due to a reduction in collisional line-broadening. Thus, the

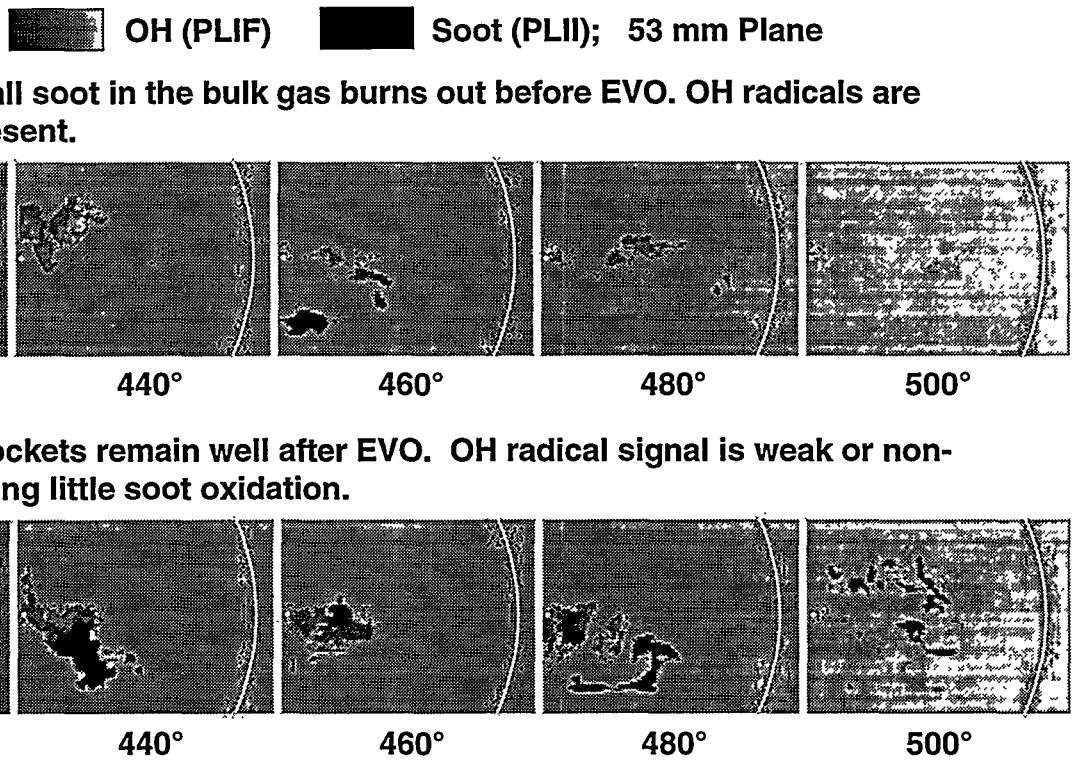

Figure 6. Temporal sequences of simultaneous OH and soot images at normal timing for 0% and 10% N_2 addition for the case of high load (C/F = 31), 1680 rpm.

actual rate of OH-concentration decrease with time is faster than it appears in the image sequences presented.

Through the rest of the 10%-N_2 sequence, the soot levels decrease, but there is still a significant amount of soot present in the bulk gas near the time of EVO at 490° as evident in the 480° and 500° images. OH is present as late as 480°, indicating that some soot oxidation continues to this crankangle. However, these oxidation rates are expected to be fairly low since the OH signal levels are quite low, suggesting lower diffusion-flame and product-gas temperatures in addition to lower OH concentrations. As a result, a significant amount of bulk-gas soot remains when combustion reactions end, as indicated by the absence of detectable OH. This is evident in the 500° image and for the large pocket of soot in the lower center of the 480° image. Accordingly, some engine-out soot emissions would be expected due to incomplete bulk-gas burnout, even for normal timing, when 10% N_2 diluent is added.

The combined effect of 11.5°-retarded timing and 10% N_2 is shown in the image sequence at the bottom of Fig. 7. For comparison, the 0%-N_2 retarded-timing sequence is shown at the top of this figure. As evident in the figure, the combination of these two NO_X-reducing techniques dramatically decreases the bulk-gas soot burnout. Although the presence of OH as late as 500° indicates that combustion sometimes continues even after EVO, there is little detectable OH in most images. Substantial bulk-gas soot remains in the 480° and 500° images suggesting that significant engine-out soot emissions will occur as a result of incomplete bulk-gas soot burnout.

Comparison with Exhaust Soot Measurements

The image-data in Figs. 4-7 suggest that incomplete soot burnout in the bulk gas is likely to be a major contributor to engine-out soot emissions. In order to obtain a better measure of the correlation between the in-cylinder and engine-out soot, a semi-quantitative analysis

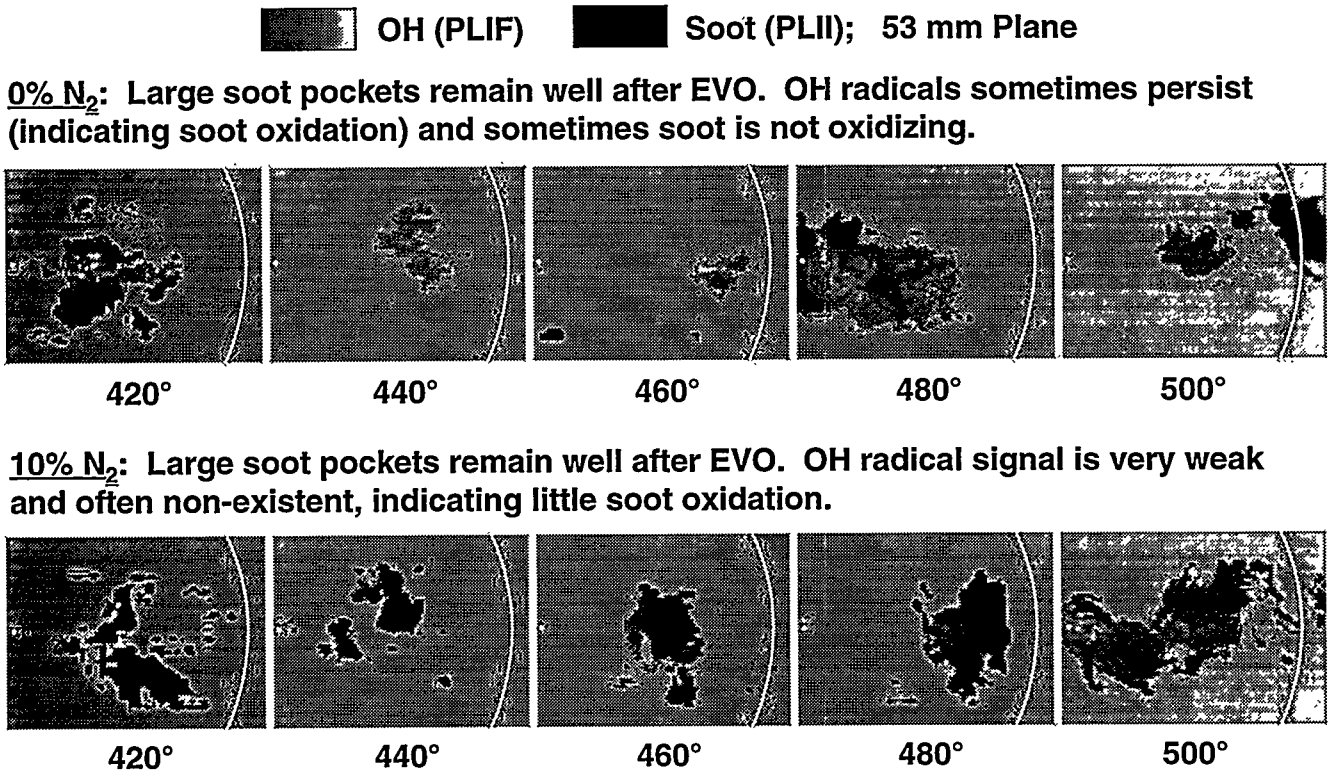

Figure 7. Temporal sequences of simultaneous OH and soot images at retarded timing for 0% and 10% N_2 addition for the case of high load (C/F = 31), 1680 rpm.

was made of the PLII-soot image data and compared with engine-out, soot-filter measurements. These engine-out measurements were made using a standard Bosch-smoke-type technique whereby the exhaust soot-mass fraction was determined from the relative darkness of a filter paper [9]. This type of exhaust soot measurement was used because it is a measure of the dry-soot component of the regulated particulate emissions, which is the component resulting from combustion-produced soot.

A semi-quantitative number corresponding to the unburned bulk-gas soot was obtained from the PLII image data as follows. First, since the PLII signal is (to first order) proportional to the volume of soot within the probe volume [6], a number proportional to the total soot within each image was obtained by integrating the PLII signal over the field of view. To account for cycle-to-cycle variation, this process was repeated for each of the 12 or 24 images taken at each crankangle, and the values were averaged together. This process was then repeated for each crankangle at which images were acquired (10° to 20° intervals). Next, a cubic spline curve was fit to these PLII intensity values to obtain a smooth curve of the ensemble-average PLII intensity with crankangle. Finally, this curve was integrated from 460° until after the last late-combustion soot was detected at 550° to obtain a measure of the total soot remaining from incomplete burnout in the bulk gas.

It should be noted that this bulk-gas soot number is only an approximation to the actual unburned bulk-gas soot for three main reasons. First, the current optical setup was designed to determine the relative spatial distributions of OH and soot, and as a result, the probe volume (defined by the laser sheet) is only a small fraction of the total in-cylinder volume. Second, in-cylinder flows appear to bring the burning soot pockets in and out of this probe volume, providing more signal at some crankangles than others. Note that for the retarded-timing case in Fig. 5, the signals become very weak at 440° and 460° and then get stronger again at 480°. Third, the soot within the probe volume is often still burning at 480° and 500° which is just before and just after EVO at 490°. It is likely that some of this soot will be further consumed before it exits the cylinder. For these reasons, it is not possible to determine an exact number for the amount of bulk-gas soot escaping combustion from the current data. However, the above method should provide satisfactory relative numbers for investigating trends between the operating conditions.

Figure 8 shows the comparison of the engine-out soot measurements with the integrated PLII measurement of the remaining bulk-gas soot. The 1200 rpm data in Fig. 8 is for a 1200 rpm high-load (C/F = 31) condition for which images were not presented. The 1200 rpm, medium-low load (C/F = 65) case from Fig. 4 is not shown because both the integrated-PLII and the exhaust-soot values were essentially zero for both normal and retarded timing.

Despite the approximate nature of the integrated PLII data, Fig. 8 shows a strong correlation between the bulk-gas and engine-out measurements. For every case, retarding the timing produces an increase in both the remaining bulk-gas and engine-out soot. Also,

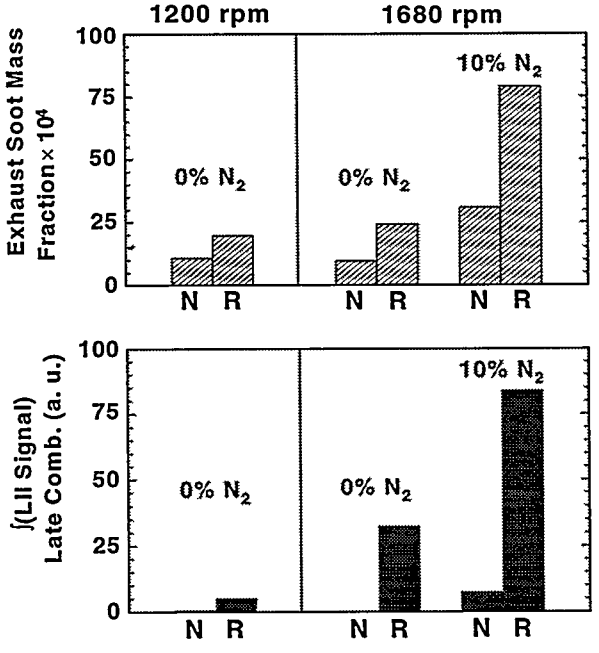

Figure 8. Comparison between engine-out (top) and late-combustion bulk-gas (bottom) soot measurements. The engine-out data were derived from Bosch-smoke-type measurements, and the late-combustion bulk-gas soot values were obtained from the PLII-soot image data in the 53 mm plane.

the addition of 10% N_2 diluent increases the soot levels obtained with both measurements for both normal and retarded timing. Finally, the combination of 10% N_2 and 11.5° timing-retard produces a substantial increase in soot levels by both measurements. These data strongly suggest that the changes in engine-out soot typically observed with timing retard and diluent addition (*e.g.* EGR) are related to changes in the bulk-gas-soot burnout rate.

The data in Fig. 8 also suggest that another pathway contributes a baseline soot emission in this research engine. For both of the normal-timing cases without diluent, the PLII data show almost no soot left in the bulk gas,[3] while engine-out measurements still indicate soot emissions. Also, for 10% N_2, the PLII data show that the bulk-gas soot with normal timing is approximately a factor of ten less than with retarded timing, while for the exhaust measurement this factor is only about three. A secondary source of soot, unrelated to the bulk-gas burnout, would explain these discrepancies. For example, soot trapped in the ring-pack then released, or deposited on in-cylinder surfaces and then stripped off could produce soot emissions even when all the bulk-gas soot is consumed. It could also add to the bulk-gas-produced soot to bring the factor between the normal and retarded timing cases with 10% N_2 in line with the exhaust measurements. However, it should be noted that the secondary soot source which appears to be affecting this research-engine data might not occur in production engines since they have different ring-pack designs than our research engine. In addition, production engines often show very low engine-out soot emissions for operating conditions comparable to our normal-timing case, more comparable with the PLII bulk-gas measurements.

[3] The data in Fig. 8 are for the 53 mm plane; however, higher elevations were also examined, and no significant bulk-gas soot was found after 420° for these conditions. Also, the normal-timing images in Fig. 5 show that almost all the soot is gone from the 53 mm plane by 420° when the piston has just moved below this elevation, so it is unlikely that any significant soot exists below this elevation at later crankangles. Similar results were found for the high-load, 1200 rpm case reported in Fig. 8.

SUMMARY AND CONCLUSIONS

An investigation of late-combustion soot burnout in a DI diesel engine has been conducted using simultaneous planar imaging of the OH-radical and soot distributions. These simultaneous images, obtained with a dual-laser, dual-camera system, show the spatial relationship between the remaining hot reaction zones and the remaining bulk-gas soot during the final stages of the combustion event. OH and soot distributions were mapped out for a variety of operating conditions, including variations in injection timing, fuel load, engine speed, and diluent addition (simulated EGR). The data show significant variations in the late-combustion burnout of soot in the bulk gas (*i.e.* away from the combustion chamber walls) with changes in operating conditions that lead to the following conclusions.

1. During the late stages of combustion, the remaining soot pockets and combustion zones tend to follow the piston down rather than expanding uniformly.
2. There is a strong correlation between incomplete soot burnout in the bulk gas and exhaust soot emissions. Both the late-combustion bulk-gas and engine-out soot levels increase with increased fuel loading, retarded injection timing, and the addition of N_2 diluent (a surrogate for EGR). This correlation suggests that incomplete burnout in the bulk gas is a major contributor to the increased soot emissions typically observed with timing sweeps and the addition of diluent.
3. The simultaneous OH and soot images show that incomplete burnout in the bulk gases can result from two causes: 1) insufficient time to complete combustion before exhaust valve opening; and 2) extinction of the combustion reactions at the periphery of remaining soot pockets. The latter is particularly prevalent with diluent addition, and the data indicate that reduced combustion and product-gas temperatures are the likely cause.
4. The data suggest that there is also a secondary source of soot emissions in this research engine. It is unclear whether this occurs in production-type engines, and additional research is needed to better understand the other pathways to soot emissions.

ACKNOWLEDGMENTS

The authors would like to thank Russell Durrett of Cummins Engine Co. for providing production-type engine emissions data and for valuable discussions that helped guide the direction of this investigation. We are also particularly grateful to Eldon Porter for maintaining and repairing the research engine and for help with the data acquisition.

This work was performed at the Combustion Research Facility, Sandia National Laboratories, Livermore, CA. Support was provided by the U.S. Department of Energy, Office of Heavy Vehicles Technologies through a cooperative research and development agreement (CRADA) with the Cummins Engine Co., Caterpillar, Inc., and Detroit Diesel Corp.

REFERENCES

1. Dec, J. E., "A Conceptual Model of DI Diesel Combustion Based on Laser-Sheet Imaging," *SAE Transactions*, Vol. 106, Sec. 3, pp. 1319-1348, paper no. 970873, 1997.
2. Heywood, J. B., Internal Combustion Engine Fundamentals, McGraw-Hill, New York, 1988.
3. Espey, C. and Dec, J. E., "Diesel Engine Combustion Studies in a Newly Designed Optical-Access Engine Using High-Speed Visualization and 2-D Laser Imaging," *SAE Transactions*, Vol. 102, Sec. 4, pp. 703-723, paper no. 930971, 1993.
4. Kittelson, D. B., Ambs, J. L., and Hadjkacem, H., "Particulate Emissions from Diesel Engines – Influence of In-Cylinder Surface," *SAE Transactions*, Vol. 99, Sec. 3, paper no. 900645, 1990.
5. zur Loye, A. O., Siebers, D. L., McKinley, T. L., Ng, H. K., and Primus, R. J., "Cycle-Resolved LDV Measurements in a Motored Diesel Engine and Comparison with k-ε Model Predictions," *SAE Transactions*, Vol. 98, Sec. 3, pp. 1142-1158, paper no. 890618, 1989.
6. Melton, L. A., "Soot Diagnostics Based on Laser Heating," *Applied Optics*, Vol. 23, No. 13, pp. 2201-2208, 1984.
7. Dec, J.E. and Canaan, R. E., "PLIF Imaging of NO Formation in a DI Diesel Engine," SAE paper no. 980147, *SAE Transactions*, in press, 1998.
8. Flynn, P. F., Durrett, R. P., Hunter, G. L., zur Loye, A. O., Akinyemi, O. C., Dec, J. E., and Westbrook, C. K., "Diesel Combustion: An Integrated View Combining Laser Diagnostics, Chemical Kinetics, and Empirical Validation," SAE paper no. 1999-01-0509, 1999.
9. Homan, H. S., "Conversion Factors among Smoke Measurements," *SAE Transactions*, Vol. 94, Sec. 2, pp. 2.533-2.547, paper no. 850267, 1985.